2018 IEEE Intelligent Vehicles Symposium (IV)
Changshu, Suzhou, China, June 26-30, 2018

Accurate Localization in Underground Garages via Cylinder Feature based Map Matching

Zhongxing Tao[1,2], Jianru Xue[1,†], Di Wang[1], Shuyang Zhang[1], Dixiao Cui[1] and Shaoyi Du[1]

Abstract— **Autonomous driving in underground garages usually utilizes a 2D/3D occupancy map for localization. However, the real scene is changing, and may not be consistent with the map. Vehicles and other objects not contained in the map are considered as obstacles, which increase the difficulty of localization and affect the accuracy of result. In this paper, we propose a cylinder rotational projection statistics(Cy-RoPS) feature descriptor, which is a local surface feature descriptor to improve the accuracy of localization. The local surface feature motivated by RoPS feature is invariant to rotation of point set enclosed in a cylinder. We also propose to employ the local surface feature for localization in a real underground garage. The experimental results show that the proposed method is robust to dynamic obstacles in the underground garage, and has a higher accuracy in localization, compared with the state-of-the-art methods.**

I. INTRODUCTION

GPS signal is usually unavailable in underground garages. The ability to park autonomously is one of the challenging problems for intelligent vehicles [1][2]. Although localization methods in indoors have been developed, but it is nontrivial or not accurate enough to be applied to autonomous parking in underground garages. To provide accurate localization, camera mounted in the parking lot and vehicle-to-infrastructure communication techniques are employed in underground garages [3]. A magnetic nail localization method was also addressed in [4]. However, these two methods are required to establish a complete infrastructure system, while many underground garages can not meet with this requirement.

3D LiDAR is widely used in autonomous driving, as its reliability is high in navigation and localization. The 3D point clouds captured by 3D LiDAR are illustrated in Fig.1, the closer the range is, the denser and more accurate the points are. In general, KF/EKF/PF filters are fusing with GPS, IMU, LiDAR, camera and other sensors for localization [2][5][6], among which GPS is usually adopted for global localization. However, GPS signal is not always available since the signal blockage happens frequently due to high buildings in urban scenes. In order to navigate in urban scenes, the vehicle requires precise localization and a priori 3D map. At the same time, the map-aided method is susceptible to dynamic obstacles in GPS denied zone, which can affect the localization performance. To overcome the problems, robust methods based on local surface feature matching are developed [5][7]. The core idea of these solutions is to detect the landmarks of environments including curbs, buildings, pillars, and walls, then the vehicle poses are estimated via landmark based map matching.

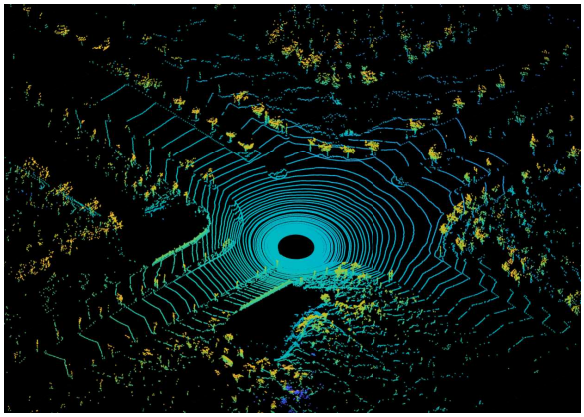

Fig. 1. LiDAR points from Velodyne HDL-64E S3, in a typical urban scene.

Several local surface feature based methods were proposed for 3D object recognition. For instance, Johnson et al. proposed Spin-Image feature [8] for efficient object recognition in cluttered 3D scenes, but its performance is sensitive to mesh resolution. Guo et al. proposed a 3D local surface descriptor, named rotational projection statistics (RoPS) feature for object recognition [9], FPFH [10] proposed by Radu et al., describes the local geometric feature around a key point, and is widely used in robotics together with PCL [11]. These local surface features are presented as a key point, and a feature descriptor computed with its neighbours.

Motivated by local surface feature based 3D object recognition method [9], we propose a cylinder rotational projection statistics feature (Cy-RoPS), and a Cy-RoPS feature based map matching method for accurate localization in underground garages. Being different from the local surface feature for 3D object recognition, our Cy-RoPS feature is used for selecting valid corresponding points in cluttered scenes, since only the valid points can improve the accuracy of localization.

The contributions of this paper are two folds: 1) we propose a Cy-RoPS feature descriptor, which is extracted from the raw LiDAR data automatically. 2) we propose an efficient Cy-RoPS based map matching method, which is

*This work was supported by the National Key R&D Plan under Grant No. 2016YFB1001004, NSFC projects 61751308 and 61773311.

[1]Visual Cognitive Computing and Intelligent Vehicle Lab, Institute of Artificial Intelligence and Robotics (IAIR), Xi'an Jiaotong University, Xi'an, P.R.China. Corresponding author's email: jrxue@mail.xjtu.edu.cn

[2]College of Physics and Electronic Engineering, Northwest Normal University, Lanzhou, P.R.China.

efficient in detecting pillars, walls, and vehicles in underground garages, and improves the accuracy of localization. The landmarks selected by Cy-RoPS include pillars and walls, which significantly increase the robustness of the map matching process. The experimental results show that our method based on Cy-RoPS feature outperforms other four state-of-the-art methods.

The rest of this paper is organized as follows. In Section II, we introduce the Cy-RoPS feature in detail. The localization with Cy-RoPS is presented in Section III. Experiments are designed for evaluating the proposed method in Section IV. Finally, we conclude the work and present the future work in Section V.

II. Cylinder Feature

Extracting Cy-RoPS involves points falling into a cylinder, which is different from other feature using sphere shape [9]. There are many columnar objects in real traffic environment, such as trees on road, pillars in underground garages, etc. Accordingly, cylinder feature has the potential to increase the discriminability in localization for autonomous parking in underground garages. We present the Cy-RoPS from the following three aspects: 1) the local coordinate system definition, 2) the feature descriptor extraction, 3) the similarity between two feature descriptors.

A. The Local Coordinate System

We denote all points enclosed in a cylinder as a point set P_s, the center of the cylinder is denoted as $\mathbf{p}_s$, which is chosen randomly, or using other method [9], as shown in Fig.2. A point belonging to P_s is denoted as $\mathbf{p}_i \in P_s$, and $\mathbf{p}_o$ is the center of the bottom plane of the cylinder, which satisfies the condition $\mathbf{p}_o = [\mathbf{p}_s(x), \mathbf{p}_s(y), l]$. P_s is selected under the constraint $d_{xy} \in (0, r]$ and $d_z \in Z$, where d_{xy} denotes the projected distance on $x-y$ plane, and d_z denotes the distance on $x-z$ and $y-z$ plane. $Z \in [l, h]$ denotes the height range of the cylinder, in this paper, we set the value between -2.0m to 0.5m for detecting pillars and walls. The kd-tree is employed for fast neighbourhood searching.

Subsequently, a local coordinate system $F_{\mathbf{uvw}}$ is defined on $\mathbf{p}_s$ with its normal $\mathbf{n}_s$ and $\mathbf{w}$, which are estimated via PCA method [12]. $\mathbf{n}_s$ is approximately equal to the eigenvector associated with the minimum eigenvalue. To eliminate the normal sign disambiguation, we set LiDAR's physic center $\mathbf{o}$ as a viewpoint for re-orienting normal when it satisfies the constraint in Eq(1).

$$\mathbf{n}_s = -\mathbf{n}_s \quad \text{when} \quad \langle \mathbf{o} - \mathbf{p}_s, \mathbf{p}_s \rangle < 0. \tag{1}$$

The vector $\mathbf{w}$ represents the principal axis of P_s distribution. Actually, $\mathbf{w}$ can be considered perpendicular to the $x-y$ plane of the LiDAR coordinate system $F_{\mathbf{xyz}}$ on the assumption that the real road surface is flat.

$$\mathbf{w} = [0,0,1], \mathbf{v} = \frac{\mathbf{n}_s \times \mathbf{w}}{\|\mathbf{n}_s \times \mathbf{w}\|}, \mathbf{u} = \frac{\mathbf{w} \times \mathbf{v}}{\|\mathbf{w} \times \mathbf{v}\|}. \tag{2}$$

Once the local coordinate system is defined, the center point and its neighbors are transformed from local coordinate system $F_{\mathbf{uvw}}$ to LiDAR coordinate system $F_{\mathbf{xyz}}$ in Fig.2 with a transformation $\mathbf{T}_c = F_{\mathbf{xyz}} \cdot F_{\mathbf{uvw}}^{-1}$, which is crucial to achieve rotation invariance.

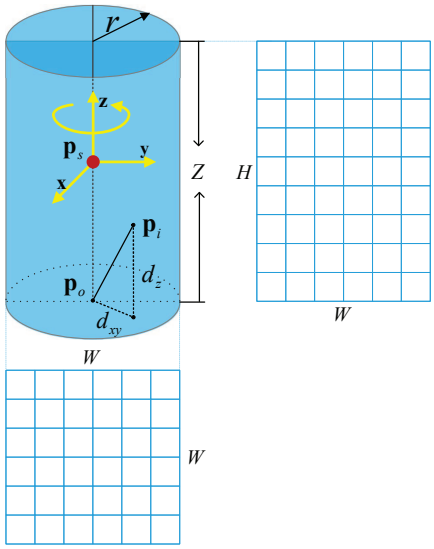

Fig. 2. Cylinder based local surface feature, and the definition of the local coordinate system.

B. The Local Surface Feature Descriptor

In this section, the local surface feature descriptor is computed by calculating statistic information of the projection of the point set. Initially, the projection is performed by rotating a fixed angle around $\mathbf{z}$ axis in LiDAR coordinate system, and subsequently all points $\mathbf{p}_i \in P_s$ are projected onto $x-y$, $x-z$, $y-z$ plane, respectively. Then, each plane is considered as a 2D projection image $\mathbf{I}(i,j)$, where $W \times H$ is employed for $x-z$ and $y-z$ plane, and $W \times W$ is used to $x-y$ plane. The pixel value of the projection image is the number of points falling into corresponding grid. That is, $\mathbf{I}(i,j)$ represents the distribution of all points in a cylinder. Obviously, the projection image provides statistical information of the P_s.

In order to enrich the rotation invariance of descriptor information, RoPS is calculated by rotating around the x, y, z axis by a series of angles [9]. Specifically, only one axis rotation projection statistical information is computed in our proposed method due to the cylinder property which is only rotated around the center line. Next, the central moments and Shannon entropy of $\mathbf{I}(i,j)$ are calculated. μ_{mn} denotes the central moment in Eq(3).

$$\mu_{mn} = \sum_{i=1}^{W} \sum_{j=1}^{L} (i-\bar{i})^m (j-\bar{j})^n \mathbf{I}(i,j), \tag{3}$$

where $\bar{i} = \sum_{i=1}^{W} \sum_{j=1}^{L} i \cdot \mathbf{I}(i,j)$, $\bar{j} = \sum_{i=1}^{W} \sum_{j=1}^{L} j \cdot \mathbf{I}(i,j)$, and $L \in \{W, H\}$ denotes the height of $\mathbf{I}(i,j)$. The Shannon entropy e can be obtained from Eq(4).

$$e = -\sum_{i=1}^{W} \sum_{j=1}^{L} \mathbf{I}(i,j) \log(\mathbf{I}(i,j)). \tag{4}$$

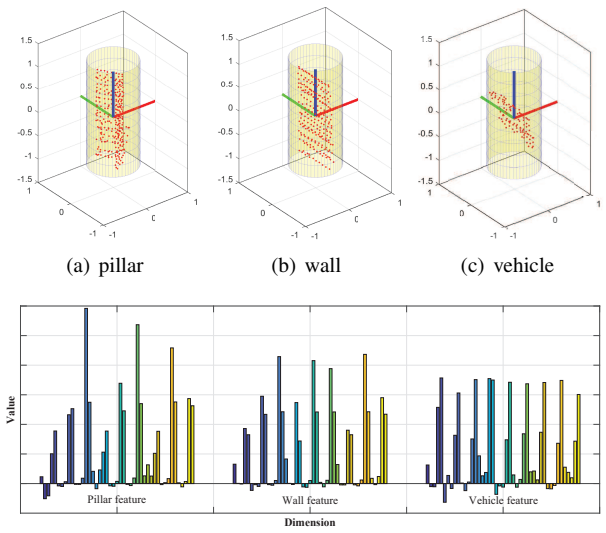

(a) pillar (b) wall (c) vehicle

(d) Feature of above three shapes

Fig. 3. The figure depicts three typical shapes in underground garages, and their Cy-RoPS features are extracted for building feature map. Actually, the mean of Cy-RoPS features of all the pillars in the training data is obtained as a feature map, similarly, the feature map of the wall and the vehicles are calculated. (a) Typical shape of a pillar in a real underground garage, the line in red, green, and blue are three axis of the LiDAR coordinate system. (b) The shape of a wall. (c) Partial shape of a vehicle. (d) Features of the above three typical shapes.

Fig.3 shows that Cy-RoPS feature is efficient in distinguishing walls, cylinders, vehicles, and others. Meanwhile, it also implies that the feature descriptor is quite different from each other. The lines in red, green and blue are three axises x, y, z, respectively. The feature descriptor generated by only rotating around the z axis is due to the cylinder characteristic. $\mathbf{F}_{xy}$, $\mathbf{F}_{xz}$, $\mathbf{F}_{yz}$ are calculated after rotating P_s by a fixed angle. More detailed steps are presented in Algorithm 1.

C. The Feature Similarity

Cosine similarity is introduced for measuring the difference of two features, which can be derived as follows:

$$d\left(\mathbf{F}_1,\mathbf{F}_2\right)=\frac{\mathbf{F}_1\cdot\mathbf{F}_2}{\|\mathbf{F}_1\|\,\|\mathbf{F}_2\|}, \tag{5}$$

where $\mathbf{F}_1$, $\mathbf{F}_2$ are two feature descriptors, the result d ranges from -1 to 1. The closer to 1, the more similar. We denote a feature descriptor as $\mathbf{F}_x$, and $\mathbf{F}_v$, $\mathbf{F}_c$, $\mathbf{F}_w$ denotes vehicle, cylinder, and wall feature, respectively. With a feature map $\mathbf{F}_{MAP}=\{\mathbf{F}_v,\mathbf{F}_c,\mathbf{F}_w\}$, the similarity between a pair of feature descriptors is computed according to Eq(5), D in Eq(6) is the set of similarities between $\mathbf{F}_x$ and $\mathbf{F}_{MAP}$.

$$D=\left\{d\left(\mathbf{F}_x,\mathbf{F}_v\right),d\left(\mathbf{F}_x,\mathbf{F}_c\right),d\left(\mathbf{F}_x,\mathbf{F}_w\right)\right\}. \tag{6}$$

III. Localization with Cy-RoPS

In this section, a localization method based on Cy-RoPS feature is presented. A detailed implementation is illustrated in Algorithm 2. It consists of two modules: 1) Valid points are selected for improving localization accuracy, which starts from Step 1 to Step 7; 2) Map matching via registration the point set P_{Eff} with the 3D occupancy map, which starts form Step 8 to Step 9.

Algorithm 1 Cy-RoPS Extraction

Input: Points in a cylinder $\mathbf{p}_i \in P_s$, Center point $\mathbf{p}_s$.
Output: Local surface feature $\mathbf{F}$.

```
Normal estimate for p_s: n_s.
Build local coordinate system F_uvw.
Transform to local coordinate via T_c = F_xyz · F_uvw^{-1}.
for each θ_j ∈ {θ_1, θ_2, θ_3} do
    p_i ∈ P_s rotate by angle θ_j.
    Project to xy plane, evenly divided into W × W bins.
    Calculate the moment and Shannon entropy
    F_xy = {μ_11, μ_12, μ_21, μ_22, e}.
    Project to xz plane, evenly divided into W × H bins.
    Calculate the moment and Shannon entropy
    F_xz = {μ_11, μ_12, μ_21, μ_22, e}.
    Project to yz plane, evenly divided into W × H bins.
    Calculate the moment and Shannon entropy
    F_yz = {μ_11, μ_12, μ_21, μ_22, e}.
    Concatenate all sub-features F = F ∪ {F_xy, F_xz, F_yz}.
end for
return F.
```

A. Selecting Valid Points

A successful localization may involve only a small portion of points, thus it is not necessary to perform matching with all points. Therefore, high quality points representing the structure of underground garages, e.g. walls, pillars, should be used for localization. Points are selected via computing the maximum similarity between local surface feature and the feature map. The maximum similarity $d_{\max}$ and the corresponding label l are obtained from Eq(7), where l is the label of object, and D is a set of similarities in Eq(6).

$$\langle l, d_{\max}\rangle = \arg\max D. \tag{7}$$

The selection procedure is formulated as Eq(8), where τ is a similarity threshold, and it is set to 0.9 in experiments. Points which dissatisfy with the constraint in Eq(8) are removed to eliminate ambiguous points belonging to obstacles.

$$\begin{array}{llll} if & d_{\max}>\tau \& l=1 & cylinder, \\ if & d_{\max}>\tau \& l=2 & wall, \\ if & d_{\max}>\tau \& l=3 & vehicle. \end{array} \tag{8}$$

P_c, P_v, P_w, P_{others} are defined as pillars, vehicles, walls, and other points, respectively. Therefore, the final chosen points P_{Valid} are obtained:

$$P_{valid}=\left(P_c\cup P_w\right)-\left(P_v\cup P_{others}\right). \tag{9}$$

More specifically, in Step 1 in Algorithm 2, the Gaussian process regression(GPR)[1] [13] is employed to divide the point clouds into a road point set P_{Grd} and a non-road point set P_{NoGrd}. The road point set will always be reserved as the main information for improving estimation accuracy

[1]https://github.com/DrGabor/LiDAR

of roll and pitch, since they provide sufficient horizontal information. In Step 4, Cy-RoPS features are calculated based on non-road point set P_{NoGrd}, which mainly includes pillars, walls, vehicles, and pedestrians. In Step 6, among the non-road points, only points falling on the pillars or walls are used to improve the accuracy of localization. Next, the point set P_{Eff} is obtained, which is high quality and uneven distributed.

Algorithm 2 Localization

Input: LiDAR points: $P = \{\mathbf{p}_i\}_{i=1}^{N_p}$;
3D Map: $Q = \{\mathbf{q}_j\}_{j=1}^{N_q}$; Initial pose $\mathbf{T_0}$;
Cylinder feature map : $\mathbf{F}_{MAP} = \{\mathbf{F}_v, \mathbf{F}_c, \mathbf{F}_w\}$;
Output: Fine pose result $\mathbf{T}$;
1: Ground segment with GPR, P_{Grd} and P_{NoGrd};
2: Center points are chosen by random selection $P_k = \{\mathbf{p}_s\}_{s=1}^{N_k} \subset P_{NoGrd}$;
3: Search all points P_s in a cylinder around $\mathbf{p}_s$ with support radius r and height threshold Z ;
4: Calculate all Cy-RoPS features $\{\mathbf{F}_s\}_{s=1}^{N_k}$;
5: Classify points via similarity measure P_c, P_w, P_v, P_{others}
6: Obtain valid points P_{Valid} via Eq(9)
7: Generate all valid points $P_{Eff} = P_{Ground} \cup P_{Valid}$;
8: Down sample points with same resolution, get P_{Reg};
9: Map Matching $\mathbf{T}(P_{Reg}, Q, \mathbf{T}_0)$;
10: **return** $\mathbf{T}$;

B. Map Matching via Registration

We obtain P_{Reg} by down-sampling P_{Eff} in Step 8 in Algorithm 2. Finally, given an initial pose $\mathbf{T}_0$, P_{Reg} is registrated with the 3D map to obtain the final localization result.

In general, a 2D occupancy grid map is sufficient in many scene, while for underground garages, 3D occupancy grid map can provide more accurate and more abundant information of pitch and roll, serving for localization in ramps or parking space detection. Moreover, the 3D occupancy grid maps have a high memory demand that grows quadratically with the scale of environments, but it is acceptable to build a 3D map since the area of underground garage is moderate. Fig.4 is the 3D occupancy grid map in our experiments, which is generated by GraphSLAM[14].

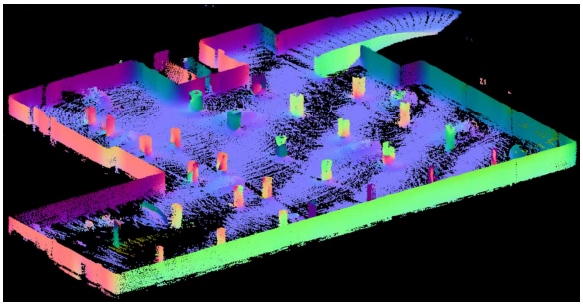

Fig. 4. 3D occupancy Map of a real underground garage.

The map matching problem here is defined as an optimization over $\mathbf{R}, \mathbf{t}$ in Eq(10) [15] [16]. $P_{Reg} = \{\mathbf{p}_i\}_{i=1}^{N_{Reg}}$ and $Q = \{\mathbf{q}_j\}_{j=1}^{N_q}$ are two point sets representing partial valid LiDAR points and 3D map in this paper, respectively. $C_{pq}(P_{Reg}, Q)$ describes the set of all correspondences, and $\{\mathbf{p}_i, \mathbf{q}_j\} \in C_{pq}$ denotes a pair of point correspondence. $\mathbf{T} = (\mathbf{R}, \mathbf{t})$ is a rigid transformation, $\mathbf{R} \in SO(3)$, $\mathbf{t} \in \mathbb{R}^3$.

$$\mathbf{T} = \arg\min_{\mathbf{T}} \sum_{\{\mathbf{p}_i, \mathbf{q}_j\} \in C_{pq}} \left\| \mathbf{q}_j - (\mathbf{R}\mathbf{p}_i + \mathbf{t}) \right\|_2^2. \tag{10}$$

In this work, we use the point-to-plane matching algorithm, which aims to minimize the error function defined as sum of squared distance between each LiDAR point and the tangent plane at its correspondence point in 3D map. It is more robust and faster than point-to-point mode [17].

IV. Experiments

In this section, the proposed method is verified in a real underground garage. Our experiments are implemented with a desktop MATLAB R2017b. All LiDAR points are collected by KUAFU autonomous vehicle which equips with a 3D LiDAR, cameras, and GPS/IMU. The experiments are carried out in two phases: 1) the performance of Cy-RoPS is evaluated in detecting pillars and walls in a real underground garage; 2) Cy-RoPS feature based map matching is tested in the underground garage.

A. Feature Detection

The results of selecting valid points including pillars and walls via Cy-RoPS feature in a real underground garage are illustrated in Fig.5. It clearly shows that Cy-RoPS works well in detecting pillars and walls in the underground garage as there is almost no any obstacle point in the point set for localization, though some distant points which are insignificant for localization are lost.

B. Localization

1) Evaluation: In this paper, we choose the root-mean-square-error (RMSE) as the metric to evaluate how close the source point is to the target point cloud. The RMSE can be formulated as Eq(11):

$$\mathrm{RMSE}(\mathbf{P}, \mathbf{Q}, \mathbf{T}) = \sqrt{\frac{1}{N_p} \sum_{i=1}^{N_p} \left\| \mathbf{q}_i - \mathbf{T}(\mathbf{p}_i) \right\|_2^2}. \tag{11}$$

Another metric is the overlapping ratio, which denotes the percentage of the successfully matched points. The larger the value is, the higher the localization accuracy achieves. The value of Ratio is calculated according to Eq(12):

$$\mathrm{Ratio} = \frac{1}{N_p} \sum_{i=1}^{N_p} s_i, \tag{12}$$

where

$$s_i = \begin{cases} 1 & d_i < \tau \\ 0 & others \end{cases},$$

$$d_i = \left\| \mathbf{q}_i - T(\mathbf{p}_j) \right\|_2.$$

where d_i represents the distance between the point $\mathbf{p}_i$ in LiDAR point cloud and the corresponding point $\mathbf{q}_j$ in 3D

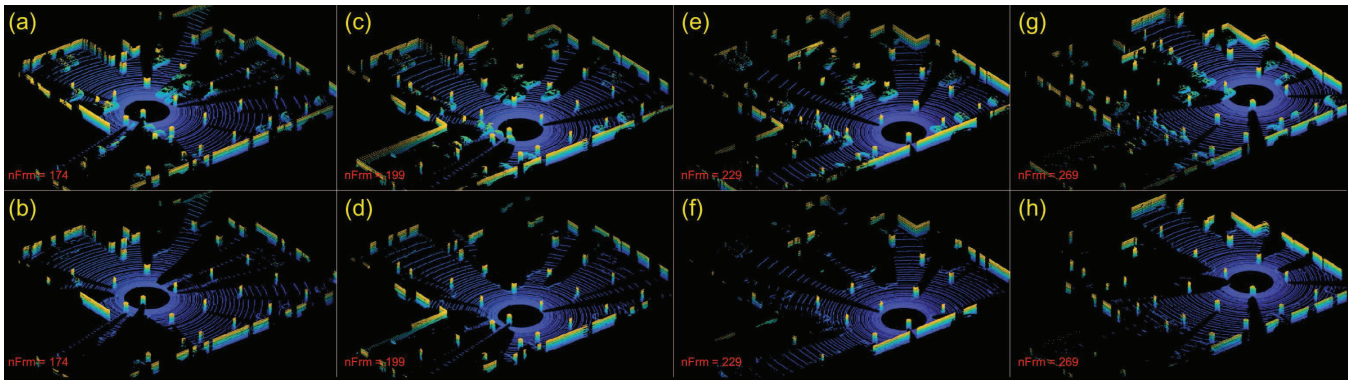

Fig. 5. The raw LiDAR points include many vehicles in (a), (c), (e), (g). And (b), (d), (f), (h) show the results of using Cy-RoPS feature to remove outliers. Our method can extract points of pillars and walls in cluttered scene.

map, s_i is a binary variable indicating whether the condition is satisfied, τ is a minimum distance threshold. It indicates that the corresponding point pair is matched successfully when the distance d_i is less than τ.

2) Experimental Settings: Localization experiments in an underground garage are performed for verifying and evaluating the performance of Cy-RoPS. Furthermore, the proposed method is compared with four state-of-the-art methods. Data sets for testing are collected in a real underground garage scenes including vehicles and other obstacles. The four methods compared with our method are:

- **CtICP**, the cost function of this method is based on the maximum correntropy criterion, which is much more robust to outliers [18].
- **IRLS**, the robust method is based on assigning different weights to different correspondences, and the problem is solved via iteratively reweighted least squares [19].
- **PL2PL**, the plane-to-plane matching method [20].
- **SparseICP**, this method avoids the outliers in LiDAR points by formulating the matching problem using sparsity inducing norms [21].

G1, G2, G3 in Tab.I are markers of three experiments, and the results are obtained using different sampling intervals of original frames in localization experiments. $\Delta\text{Frm} = 2$ in G1 means every 3 frames are used for localization, while for G2 and G3, the ΔFrm is set to 5 and 10, respectively. Different sampling intervals of frames are employed for evaluating the robustness of initial transformation for all methods. The larger the value of ΔFrm is, the coarser the initial transformation is. Moreover, the average number of LiDAR points for matching process are set around 2500 for **CtICP**, **IRLS**, **PL2PL**, **SparseICP**, and 2000 for **Ours**. With the given 3D map and initial transformations, we compared four localization systems with ours.

3) Results: The comparison is illustrated in Fig.6, Fig.7, Fig.8, which correspond to G1, G2, G3 in Tab.I. Red line represents our proposed method, and green, blue, magenta, black are four different matching methods, i.e., CtICP, IRLS, PL2PL, SparseICP respectively.

It clearly shows that our method based on Cy-RoPS feature not only improves the accuracy of localization in underground garages, but it is also more robust to different initial transformation compared with other four methods. The average evaluation results are also recorded in Tab.I. The results obviously indicates that our method achieves higher localization accuracy with even less points. Meanwhile, our method needs the shortest time for matching. In addition, the

TABLE I
RESULT OF DIFFERENT METHOD

		CtICP	IRLS	PL2PL	SparseICP	Ours
G1	RMSE(m)	0.0920	**0.0702**	0.0725	0.0732	0.0710
	Ratio(%)	0.7849	0.8360	0.8200	0.8313	**0.8367**
	Time(s)	1.5909	1.8773	4.2968	5.2648	**1.1593**
G2	RMSE(m)	0.0917	0.0790	0.0726	0.0902	**0.0709**
	Ratio(%)	0.7840	0.5787	0.8283	0.5478	**0.8366**
	Time(s)	1.9745	2.2028	4.7317	5.7769	**1.1957**
G3	RMSE(m)	0.1158	0.0798	0.0984	0.0908	**0.0710**
	Ratio(%)	0.4463	0.5563	0.4728	0.5360	**0.8371**
	Time(s)	2.3647	2.2685	5.7414	5.6110	**1.2574**

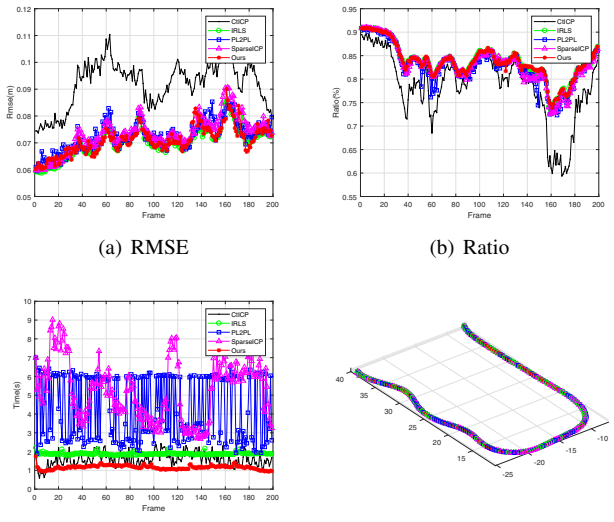

(a) RMSE (b) Ratio

(c) Time (d) Trajectory

Fig. 6. The results are obtained by setting $\Delta\text{Frm} = 2$. It clearly shows that all methods succeed in matching, our method, IRLS, and SparseICP have a better performance than PL2PL and CtICP.

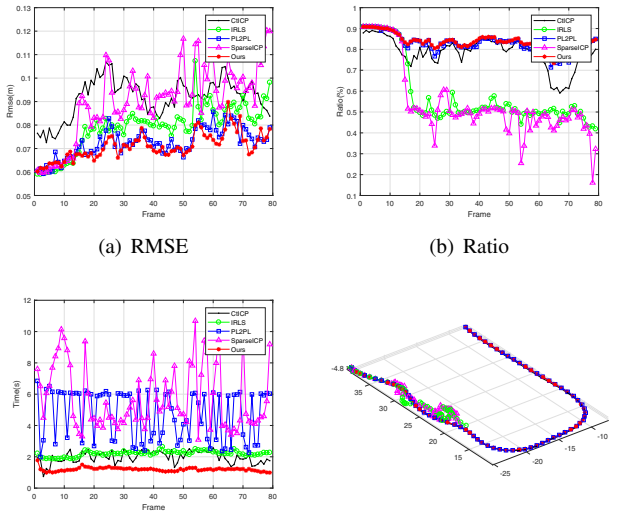

(a) RMSE (b) Ratio

(c) Time (d) Trajectory

Fig. 7. ΔFrm = 5. Our method have a higher performance by analysing the criteria of RMSE, Ratio, and Time. In addition, IRLS and SparseICP are not available from the Trajectory result.

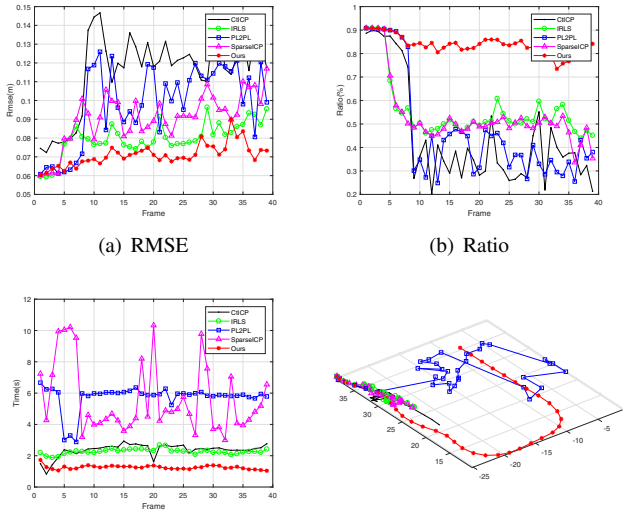

(a) RMSE (b) Ratio

(c) Time (d) Trajectory

Fig. 8. ΔFrm = 10. The results clearly indicate that our proposed method is the only successful matching method in experiment.

performance of Cy-RoPS based method is almost unaffected by the sampling interval from the Tab.I.

V. CONCLUSIONS

In this paper, Cy-RoPS feature for detecting pillars and walls in underground garages is proposed. The feature efficiently represents geometric information of the objects existing in the real traffic environment. In order to achieve accurate localization, Cy-RoPS features are employed for selecting valid points which have high quality for map matching process. The experimental results show that the proposed method can exactly select pillars and walls points and effectively improve the accuracy of localization, compared with the existing state-of-the-art methods. The accuracy of proposed localization method in underground garages is sufficient for autonomous driving, but the time consumption is uptight for real-time system, especially the road segmentation with GPR and the Cy-RoPS extraction cost the most time of computing. The future work is focused on improving the performance of the Cy-RoPS.

REFERENCES

[1] L. Cheng and T. Qiao, "Localization in the parking lot by parked-vehicle assistance," *IEEE Transactions on Intelligent Transportation Systems*, vol. 17, no. 12, pp. 3629–3634, Dec 2016.

[2] S. Wahl, P. Schlumberger, R. Rojas, and M. Stmpfle, "Localization inside a populated parking garage by using particle filters with a map of the static environment," in *2015 IEEE Intelligent Vehicles Symposium (IV)*, June 2015, pp. 95–100.

[3] A. K. T. R. Kumar, B. Schufele, D. Becker, O. Sawade, and I. Radusch, "Indoor localization of vehicles using deep learning," in *2016 IEEE 17th International Symposium on A World of Wireless, Mobile and Multimedia Networks (WoWMoM)*, June 2016, pp. 1–6.

[4] B. Park and H. Myung, "Resilient underground localization using magnetic field anomalies for drilling environment," *IEEE Transactions on Industrial Electronics*, vol. 65, no. 2, pp. 1377–1387, Feb 2018.

[5] A. Y. Hata and D. F. Wolf, "Feature detection for vehicle localization in urban environments using a multilayer lidar," *IEEE Transactions on Intelligent Transportation Systems*, vol. 17, no. 2, pp. 420–429, 2016.

[6] R. W. Wolcott and R. M. Eustice, "Visual localization within lidar maps for automated urban driving," in *Ieee/rsj International Conference on Intelligent Robots and Systems*, 2014, pp. 176–183.

[7] D. Wang, J. Xue, D. Cui, and Y. Zhong, "A robust submap-based road shape estimation via iterative gaussian process regression," in *2017 IEEE Intelligent Vehicles Symposium (IV)*, June 2017, pp. 1776–1781.

[8] A. E. Johnson and M. Hebert, "Using spin images for efficient object recognition in cluttered 3d scenes," *IEEE Transactions on Pattern Analysis and Machine Intelligence*, vol. 21, pp. 433–449, May 1999.

[9] Y. Guo, F. A. Sohel, M. Bennamoun, M. Lu, and J. Wan, "Rotational projection statistics for 3d local surface description and object recognition," *International Journal of Computer Vision*, vol. 105, no. 1, pp. 63–86, 2013.

[10] R. B. Rusu, N. Blodow, and M. Beetz, "Fast point feature histograms (fpfh) for 3d registration," in *2009 IEEE International Conference on Robotics and Automation*, May 2009, pp. 3212–3217.

[11] R. B. Rusu and S. Cousins, "3d is here: Point cloud library (pcl)," in *2011 IEEE International Conference on Robotics and Automation*, May 2011, pp. 1–4.

[12] C. Papazov, S. Haddadin, S. Parusel, K. Krieger, and D. Burschka, "Rigid 3d geometry matching for grasping of known objects in cluttered scenes," *The International Journal of Robotics Research*, vol. 31, no. 4, pp. 538–553, 2012.

[13] T. Chen, B. Dai, R. Wang, and D. Liu, "Gaussian-process-based real-time ground segmentation for autonomous land vehicles," *Journal of Intelligent and Robotic Systems*, vol. 76, no. 3, pp. 563–582, 2014.

[14] S. Thrun and M. Montemerlo, "The graph slam algorithm with applications to large-scale mapping of urban structures," *International Journal of Robotics Research*, vol. 25, no. 5, pp. 403–429, 2006.

[15] S. Du, J. Liu, B. Bi, J. Zhu, and J. Xue, "New iterative closest point algorithm for isotropic scaling registration of point sets with noise," *Journal of Visual Communication & Image Representation*, vol. 38, pp. 207–216, 2016.

[16] S. Du, J. Liu, C. Zhang, J. Zhu, and K. Li, "Probability iterative closest point algorithm for m -d point set registration with noise," *Neurocomputing*, vol. 157, pp. 187–198, 2015.

[17] K. L. Low, "Linear least-squares optimization for point-to-plane icp surface registration," *Chapel Hill*, 2004.

[18] R. He, W. S. Zheng, and B. G. Hu, "Maximum correntropy criterion for robust face recognition," *IEEE Transactions on Pattern Analysis & Machine Intelligence*, vol. 33, no. 8, pp. 1561–76, 2011.

[19] P. Bergstrm and O. Edlund, "Robust registration of point sets using iteratively reweighted least squares," *Computational Optimization & Applications*, vol. 58, no. 3, pp. 543–561, 2014.

[20] A. Segal, D. Hhnel, and S. Thrun, "Generalized-icp," 2009.

[21] S. Bouaziz, A. Tagliasacchi, and M. Pauly, "Sparse iterative closest point," in *Eleventh Eurographics/acmsiggraph Symposium on Geometry Processing*, 2013, pp. 113–123.